ISSN 1060-992X, Optical Memory and Neural Networks, 2020, Vol. 29, No. 4, pp. 269–292. © Allerton Press, Inc., 2020.

# Current Trends in Development of Optical Metrology

**O. V. Angelsky[a, b, *], P. P. Maksymyak[b], C. Yu. Zenkova[b], S. G. Hanson[c], and Jun Zheng[a]**

[a] *Research Institute of Zhejiang University, Taizhou, 310027 China*

[b] *Chernivtsi National University, Chernivtsi, 58012 Ukraine*

[c] *DTU Fotonik, Department of Photonics Engineering, Roskilde, DK-4000 Denmark*

**e-mail: o.angelsky@chnu.edu.ua*

Received May 8, 2020; revised August 3, 2020; accepted August 31, 2020

**Abstract**—This review offers the reader some of the achievements of modern optical metrology. Over the past decades, it has become possible to make a leap in the basic approaches of metrology from the nano to the femto, approaching the pico level of measurements. Control of nano (micro) particle motion by an optical field and their use for testing complex optical fields; ultra-precise determination of the optical parameters of both solid and liquid and gas-like substances by optical methods; the tiny metrology of the phase shift of orthogonally polarized beams and the determination of their degree of mutual coherence, by interference methods and many other, are proposed for consideration in this paper. Optical metrology, which is provided by three-dimensional polarization distributions of optical fields, where structured light plays a special role; by using femtosecond lasers, and much more, demonstrates the prospects of optical methods in modern measuring systems.

*Keywords:* optical metrology, nano (micro) particle, optical field, polarization, measurement

**DOI:** 10.3103/S1060992X20040025

## INTRODUCTION

Metrology is a field of scientific and technical research that has absorbed optical engineering and precision measurements, directions that intensively develop.

This is proclaimed by the world achievements in the creation of femtosecond lasers (John L. Hall and Theodor W. Hänsch "for their contributions to the development of laser-based precision spectroscopy, including the optical frequency comb technique", Nobel Prize in Physics 2005), the making and successful operation of an optical fluorescence microscope with a record resolution of 10 nanometers (Eric Betzig, Stefan W. Hell and William E. Moerner "for the development of super-resolved fluorescence microscopy", Nobel Prize in Chemistry 2014) [1], and the intensive research in the development and use of optical tweezers, manipulators, molecular motors, etc. (Arthur Ashkin "for the optical tweezers and their application to biological systems", Nobel Prize in Physics 2018).

Using the capabilities of optical observation, diagnostics, and metrology, which are opening up thanks to the evolution of modern methods for the formation of various features of structured light [2], it has become possible in a practically revolutionary way to reach the verge of a picometer level resolution of measurements.

With this resolution, to some extent, the advantages of the visible range of the spectrum are retained, i.e. the ability to visually observe the studied objects, scenes, events, scenarios, using the capabilities provided by CCD cameras that work in the IR and UV ranges.

Already today, ways of implementing metrology of optical field parameters in three-dimensional space [3–5] with nanometer resolution have been outlined. The relevance and importance of such measurements is formed in the case of study of transformations of polarized light and the possibility of implementing an ultra-high resolution in the optical range.

In general, the history of the development of this problem is as follows: The classical theory of optical phenomena, proven over the years, even for centuries, made it possible to describe, explain, predict, create well-known diverse optical systems that brilliantly proved themselves in practice and in today life. However, the current state of physics and life sciences, in general, require expanding the capabilities of optical systems by moving from the systems of the so-called millimeter-micrometer range to devices and instruments operating in the nano-, pico-, femto-level ranges.

Moreover, the preservation of the benefits of visual observation and control is a priority task here.

The implementation of such tasks is impossible without finding and discovering new technical and technological solutions, the creation of hybrid metrological systems that can simultaneously work in different spectral ranges, in particular in IR and UV areas, using different parameters of the optical radiation field for diagnostics, and evidently their interconnection.

A review of the state of research at this level is based on a platform that has been formed in a number of directions by the authors of this paper.

So, the goal of this paper is to analyze the possibilities of performing precision measurements in the picometer range, based largely on the results of own research by the authors and on the analysis of the state of the problem as a whole.

## 1. MEASUREMENT OF PHASE SHIFT BETWEEN ORTHOGONALLY POLARIZED BEAMS AT TOTAL INTERNAL REFLECTION (TIR)

We would like to start this paper by considering the problem of high-precision interference measurements of phase shift between orthogonally linearly polarized beams with Total Internal Reflection (TIR) at the interface between two dielectric surfaces.

As is known, in the case of TIR, linearly (circularly, elliptically) polarized beams, acquire some lateral (spatial—longitudinal (transverse)) displacement, that cannot be described within the framework of the geometric optics laws approximation [6, 7]. Such lateral spatial shifts can occur either in the plane of incidence, or in the direction perpendicular to this plane. Spatial lateral displacements are accompanied respectively by angular displacements of the reflected beam in the case of partial reflection and transmission. Depending on the direction of displacement, one speaks about the Goos—Henchen (GH) or Imbert—Fedorov effect (IF) [6–10]. Estimation of possible shifts is becoming increasingly actual with the development of nanooptics, the tasks of metrology and control of the optical surfaces homogeneity, as well as for evaluation of the refractive index of prism elements.

These effects, in principle, can be interpreted as the result of interference of plane waves components (with altered amplitudes and/or phases, as a result of interaction) in the reflected beam. In fact, the physical nature of these shifts is completely different. The IF shift (also called the Spin Hall (SH) light shift [6, 7, 9]) occurs due to the evolution of the geometric phase and the resulting spin-orbit interaction of light. The GH shift is connected with the angular gradient of the amplitude complex reflection/refraction coefficients ($F^r_{p,s}$) [6, 7, 9].

Let us consider the simplest case of linearly polarized beams with p- ($\vec{E}_p$) and s- ($\vec{E}_s$) polarizations (Figs. 1a, 1b). The spatial shift of these beams ($Sh_p$ and $Sh_s$, $Sh_p > Sh_s$) during reflection occurs due to the different phase change of the polarization components of the incident under their reflection at the interface between the two dielectrics. When considering the propagation process of such beams, the central component of the incident beam with the vector $\vec{k}_c$ is indicated, and the lateral components of the beam with the vectors $\vec{k}_l$, the propagation direction of which differs from $\vec{k}_c$. The change of the position of the central $\vec{k}'_c$ and lateral components of the beam $\vec{k}'_l$ under reflection in the incident plane is realized in this case. The displacement of the reflected beam in this plane is demonstrated in Fig. 1.

In a general situation, lateral components of the incident beam, propagating at the interface of two media, that are characterized by a certain spatial shift with respect to the plane of incidence [6, 7] determine that

1. the incident beam acquires insignificant ellipticity,

2. spatial deviations of the vectors $\vec{k}_l$ of the lateral beams within the plane of incidence lead to a change in the angle of incidence of the beam at the interface of the two media,

3. the deviation of the lateral beams in the perpendicular direction will determine a slight turn of the incident plane itself with respect to the normal at the interface.

The lateral (longitudinal) spatial displacements of the incidence beam, which occur in the incident plane ($Sh_p$ and $Sh_s$), are associated with the change of the angle of incidence, and determine the Goos-Hänchen effect, which can be detected under the condition of the absence of a transmitted beam. At the same time, when the Fresnel amplitude coefficients of the reflected beam $F^r_{p,s} = \exp(i\delta_{p,s})$ acquire complexities in the case of TIR, the phase shift $\delta_{p,s}$ is real-valued.

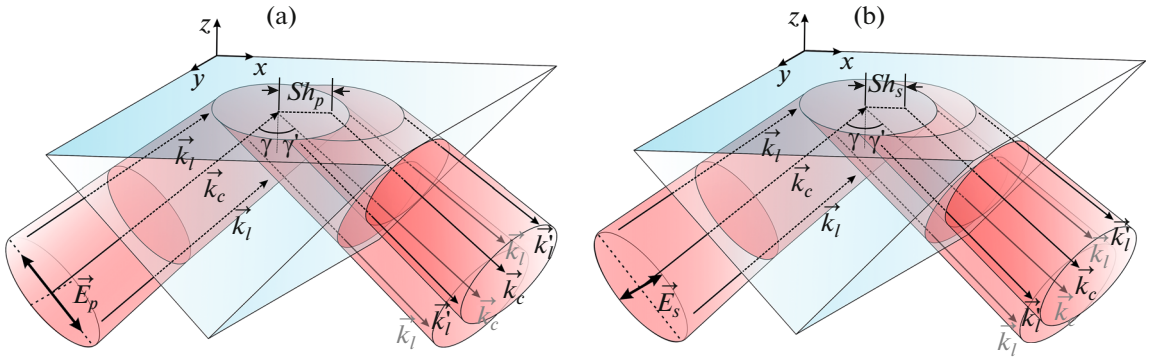


**Fig. 1.** Reflection of linearly polarized beams with p- ($\vec{E}_p$ ) and s- ($\vec{E}_s$) polarizations at two dielectrics interface. Here $\vec{k}_c(\vec{k}_l)$ determines the position of the central (lateral) components of the beams (before reflection and after reflection without shift), $\vec{k}_c'$ ($\vec{k}_l'$) determines the direction of propagation of the central (lateral) components after reflection with the shift of the beams in the incident plane. $Sh_p$ and $Sh_s$ are the corresponding shifts.

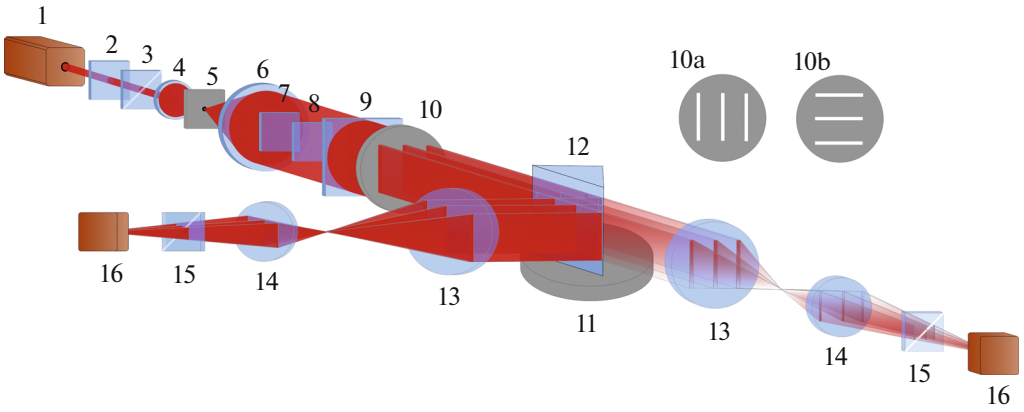


**Fig. 2.** Experimental setup: (1) single-mode He-Ne laser 1 with wavelength $\lambda = 0.6328$ μm and power $P = 50$ mW; (2, 9) quarter-wave plates; (3, 15) polarizers; (4, 14) microobjectives; (5) pinhole; (6, 13) objectives; (7) half-wave plate; (8) phase compensator; (10) diaphragm; (11) goniometer table; (12) prism; (16) CCD-camera.

The purpose of this part of the paper is to illustrate the metrology of the phase shifts of the beams in the plane of incidence under the TIR at the prism-air interface. The possibility of estimating the phase shift for *s*- and *p*-polarized beams is investigated. It is expected that since the magnitude of the shift is different for differently polarized beams, the diagnosis of such a shift can be carried out by measuring the relative phase shift between the beams with *s*- and *p*-polarizations.

It is proposed to use the interference method in a similar scheme to the classical Young scheme, to measure the phase shift between orthogonally linearly polarized beams at TIR (Fig. 2).

The source of optical radiation was a single-mode He-Ne laser 1 with wavelength $\lambda = 0.6328$ μm and power $P = 50$ mW. The quarter-wave plate (2) and linear polarizer 3 made it possible to form a linearly polarized beam with the required azimuth of polarization. High quality micro objective (4) ($3^x$), pinhole (5) (30 microns) and objective (6) ($f = 63$ cm) of the telescopic system, allow us to form a plane wave with wavefront irregularities smaller than $\lambda/20$. The plane wave is directed to diaphragm (10), which consists of three identical slits, located at exactly the same distances from each other. The slits were oriented horizontally (10a, Fig. 2) or vertically (10b, Fig. 2) due to the rotation of diaphragm (10) by 90°. Depending on the orientation of the diaphragm, the slits will be oriented either perpendicular to the plane of incidence of the beams or coincide with the plane of incidence. The image of the slits in the lens focus (13) will define the plane of interference. Diffraction by slits causes a change in the direction of propagation of the lateral components of the beam, i.e., the diffraction angle, and hence the angle of incidence at the interface. Accordingly, the value of the phase shift will be determined under the TIR at the incident plane.

Half-wave plate (7) is used to convert the polarization of the central beam into the polarization that is orthogonal to the polarization of the lateral linearly polarized beams.

Let the linearly polarized beams that propagate from the lateral slits be characterized by *s*-polarization. Then, the central beam will be characterized by *p*-polarization. For vertically oriented slits, the orientation of which coincides with the plane of incidence, a phase shift of *p*- and lateral *s*-polarized beams take place at the incident plane and appears at the interference plane of the resulting interference pattern.

Accordingly, for horizontally located slits, whose orientation is perpendicular to the plane of incidence, the contribution of phase shifts to the resulting interference distribution will be determined by the angle of inclination of the lateral components $\vec{k}_l$ for each of the three beams, caused by diffraction by the slits. This will cause almost the same phase shift of all three beams; it will not significantly change the interference distribution. An analysis of the interference pattern is also carried out in the interference plane of the lens (13) focus. Comparison of interference patterns at different slit orientations, differences in interference distributions, allow us to estimate the value of the phase shift between orthogonally polarized *s*- and *p*- beams.

Calibrated phase compensator 8 facilitates an arbitrary but controlled phase difference between the orthogonally polarized beams.

Movable quarter-wave plate (9) transforms the linearly orthogonally polarized beams into orthogonally circularly polarized beams. TIR of these three beams from the diagonal prism face 12, located on the table of goniometer (11) is enabled. The refractive index of the prism for wavelength $\lambda = 0.6328$ μm is $n = 1.515$. The flatness of the prism surfaces is supposed to be very high, and not less than $\lambda/25$.

Fraunhofer diffraction and interference of the three reflected beams are observed in the focal plane of the lens 13 ($f = 38$ cm), using a micro lens 14 and a CCD camera 16. The maximum contrast of the interference pattern was achieved for the azimuth of polarization of 45° with respect to the polarization planes of the orthogonal linearly polarized beams from polarizer 15. In the absence of prism 12, it is possible to observe the diffraction and interference of the three beams in a straight beam (shown in Fig. 2 by dashed lines), which allows one to adjust the elements of the scheme.

### *1.1. Experiment*

The results of computer simulation of the resulting intensity distribution in the interference pattern of the three beams are presented in Fig. 3. If all three beams have the same phase, the intensity distribution has the appearance presented in Fig. 3a. Any change of the phase of the central beam with respect to the lateral ones or any other arbitrary relative change of the phase between the beams causes a change of their interference distribution. Figure 3b demonstrates the intensity distribution corresponding to the situation when the central beam is phase-shifted with respect to the lateral beams by $\pi/2$. The phase shift by $\pi$ of the central beam, leads to the change of maxima and minima positions in the resulting distribution (Fig. 3c) in comparison with the initial situation.

### *1.2. Experimental Setup Calibration*

At the beginning, the calibration of the experimental setup was performed. For this purpose, we obtained an interference image in the focus of the objective in the straight beam, without plates (7 and 9), compensator 8 and prism 12 (Fig. 2).

The next Fig. 4 shows that the horizontally (a) and vertically (b) oriented interference patterns are identical and correspond to the phase equality of all three beams. This indicates that the illumination channel of the interferometer is aligned.

Next, we set plate $\lambda/2$ (7), which transforms the linear polarization of the central beam into the linear but orthogonally polarization of the lateral beams.

Different phase difference between the central and lateral beams due to the influence of the compensator leads to the change of the interference pattern (Fig. 5). We consider that the polarization of the beam propagating through the lateral slits is *s*-polarization. Then the central beam is formed with *p*- polarization. The introduction of phase compensator 8, allows us to compensate the phase shift of the central beam, which appears due to the thickness of plate ($\lambda/2$) (7) or for other reasons.

The compensator action is demonstrated in Fig. 5, which presents the interference patterns for different phase differences between the central and lateral beams.

As a reference system for the displacement of the interference fringes due to the path difference between the orthogonally polarized beams, we have taken a doubling of the frequency of the interference

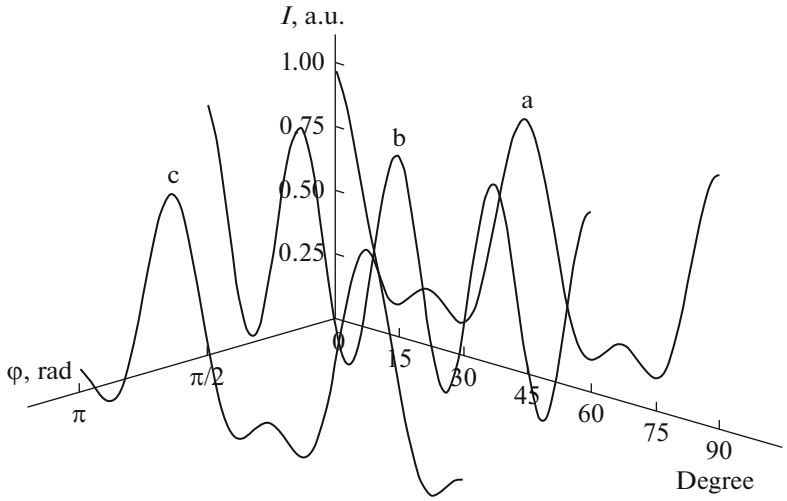


**Fig. 3.** Intensity distribution at three-beam interference for phase differences between the central and lateral beams: (a) 0; (b) π/2; (c) π rad.

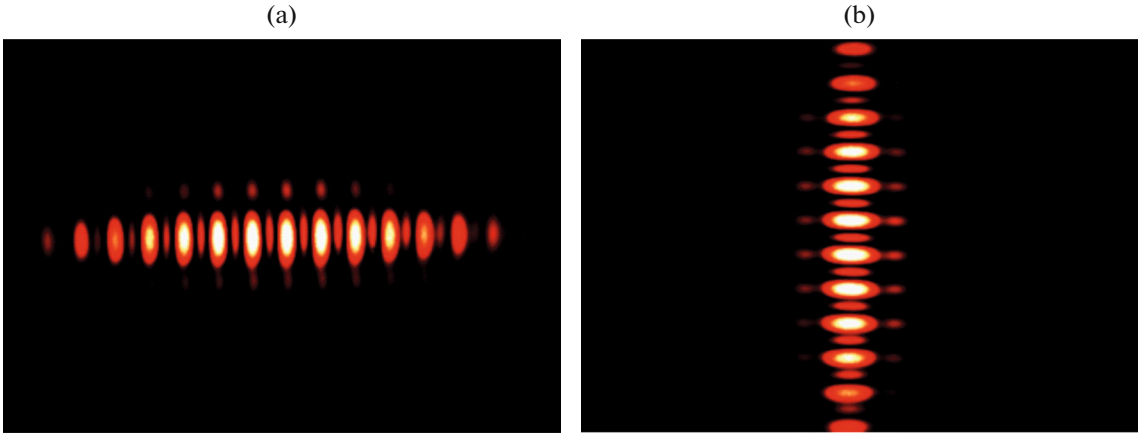


**Fig. 4.** Interference pattern in the objective focus for horizontal (a) and vertical (b) position of diaphragm 10 (Fig. 2).

fringes (Figs. 4, 5). Such a doubling can be more clearly recorded visually, and in this case there is an opportunity to automate the measurement process.

The phase shift measurement using the compensator can be carried out with an accuracy of 6′, which exceeds the required measurement accuracy of the interference fringes intensity coinciding when doubling them. The calibration of the compensator was carried out as follows: Using the measuring limb of the phase compensator, one can set the reference point when measuring the phase delay. Therefore, upon reaching a doubling of the frequency of the interference fringes (Fig. 5c), we could set the phase delay between the orthogonally polarized beams equal to 90° in the compensator limb. It was this procedure that allowed the phase compensator to be calibrated.

The phase difference between orthogonally polarized beams at TIR at our experiment is estimated by the ratio: $\delta = \delta_p - \delta_s = 2\arctan\left(\frac{\cos\theta\sqrt{\sin^2\theta - (1/n)^2}}{\sin^2\theta}\right)$, and gives a value of 0.69 rad, which is well correlated with the results obtained experimentally.

The accuracy of the path difference obtained in a three-beam interferometer (Fig. 6) is determined by the measuring accuracy of the two interference fringes intensity, which can be characterized by a relative intensity difference $\Delta I/I$. The similarity of neighboring interference fringes is about of 5%, which corresponds to an accuracy of optical path difference of $\lambda/100$ (in our case, about 6 nm).

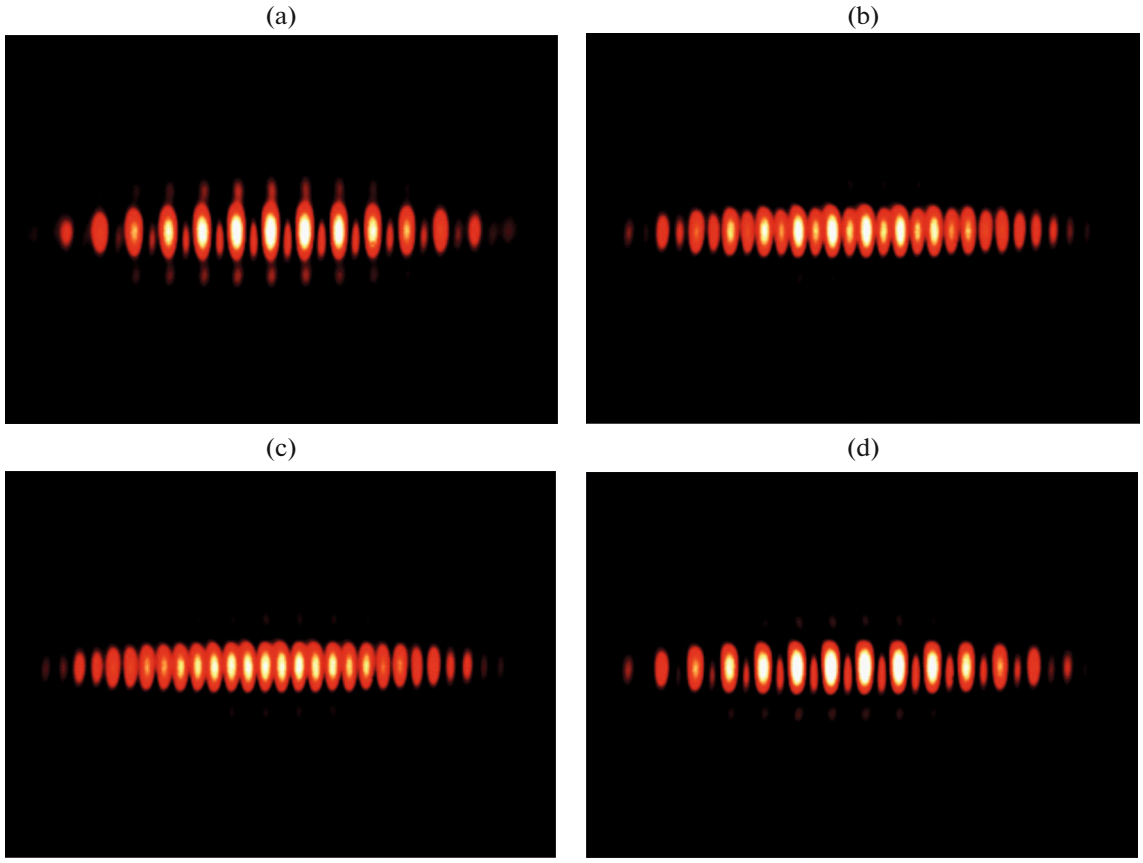


**Fig. 5.** Three-ray interference pattern for phase difference between the central and lateral beams (in radians): (a) 0; (b) $\pi/4$; (c) $\pi/2$; (d) $\pi$.

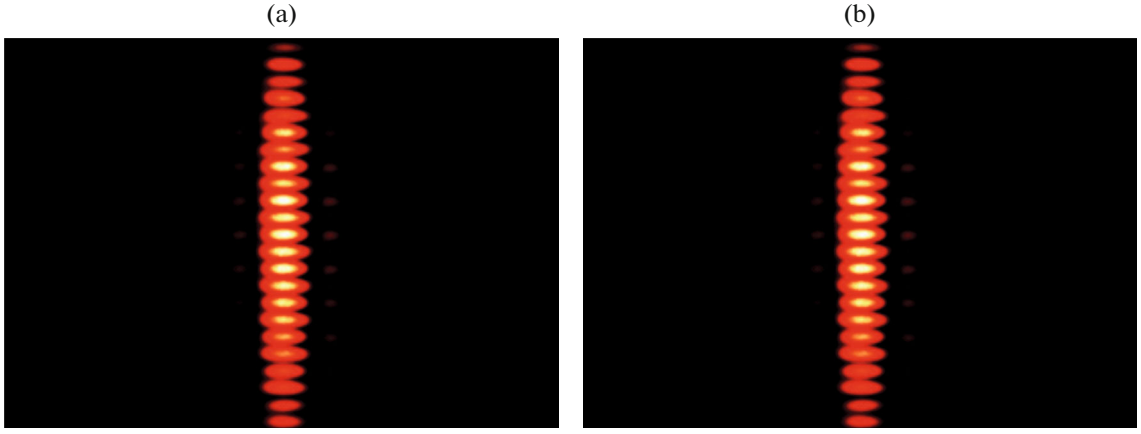


**Fig. 6.** Interference pattern of three-beam interfe rence at TIR for the vertical position of the diaphragm 10 (Fig. 2, 10b) and for its horizontal position (Fig. 2, 10a). Calibration takes place in presence of the prism.

The obtained accuracy of the optical path length determination in the presented model experiment is unique. This allows measurements in the nanometer level. In particular, the selected experimental conditions determine the precision accuracy of the estimation of not only the path length, but also the relative phase shift between the orthogonally polarized components, supporting the predicted theoretical calculations.

The achievement of the error of optical measurements at the nanometer level becomes possible when the corresponding set of parameters describing the field of optical radiation is taken into account. Evaluation of each of the parameters, studying the influence of one parameter on another, sets the condition for obtaining the high accuracy.

So, the next step in our description is to present existing approaches [11–22] of the interconnection of correlation and polarization parameters of the optical fields, for obtaining the theoretical and experimental conditions for high-precision measurement.

## 2. INTERCONNECTION OF POLARIZATION AND CORRELATION PARAMETERS OF OPTICAL FIELDS

At this step of the metrology of optical fields description, it is necessary to consider the interconnection between the degree of correlation of interacting optical beams and the quantitative indicators of the resulting polarization distributions during the qualitative and quantitative estimation of the corresponding parameter. Optical metrology approaches are being developed when it is important to take into account the beam oscillations in the longitudinal direction, providing a three-dimensional representation of the optical field [1, 3]. Here, the three-dimensional distribution of the electrical strength vector oscillation is important. Taking into account the third component of the optical field becomes relevant in the approximation in near-field optics or from the point of view of using confocal microscopy methods.

Various parameters are used to describe partially coherent and partially polarized beams, such as the degree of mutual coherence [11], the degree of coherence in the electromagnetic approximation [12], the electromagnetic degree of coherence [13, 14], and the intrinsic degrees of coherence [15]. Parameters for describing the coherent and polarization properties of the electromagnetic field inherent in the united theory of coherence and polarization were proposed by Wolf [16], introduced on the basis of a three-dimensional coherence matrix. The coherence matrix allows one to determine the degree of correlation between the orthogonal components of two superposing beams at two different points in time, and at two points in space. The last two parameters [13–15] describing the degree of coherence are invariant to the transformation of the coordinate system and can be used in situations of three-dimensional representation of the electromagnetic field, in the approximation of near-field optics, when the longitudinal component becomes actual. The value of the degree of polarization is also obtained from the coherence matrix and determines the degree of correlation of the field components at a given point in space and at a given time [17]. The introduced metrological parameters of the degree of mutual coherence of superposing beams [13–15] are sufficient and necessary in order to determine the degree of mutual correlation of superposing orthogonally polarized beams with a convergence angle of 90° (when using parameters of internal degree of coherence). However, these approaches do not cover the situation of interference [18, 19] of two superposing orthogonal beams polarized in the plane of incidence, with an angle of convergence of 90°. The absence of the intensity modulation here is accompanied by the polarization modulation and modulation of the Poynting vector occurring in the plane of incidence [20–22]. To determine the degree of coherence of such beams, we proposed a new specially introduced metrological parameter—the visibility modulation depth (relative visibility), the use of which was made possible due to the third reference wave in the three-beam interference pattern, which allowed us to form a field modulated in intensity [18, 19].

The same parameter was tested to assess the degree of correlation of circularly polarized fields of the same direction of rotation of the electrical strength vector, the convergence angle of which is 90° [23].

We use a linearly polarized plane reference wave, correlated at least with one of the two superposing waves, which is perpendicular to the registration plane. In such a way, transformation of the spatial polarization distribution of the resulting field into a periodic spatial intensity distribution has been implemented [18, 19, 24].

In other words, we consider the result of three-beam superposition for the waves polarized at the incidence plane, $\vec{E}^{(1)}$, $\vec{E}^{(2)}$ and $\vec{E}^{(3)}$; here $\vec{E}^{(3)}$—is a reference wave. Let the point $\vec{\mathrm{r}}$ define a point in the plane of registration of the field. Then, at time $t$, a random electromagnetic field at the indicated point $\vec{r}$ can be written $\vec{E} = \vec{E}^{(1)} + \vec{E}^{(2)} + \vec{E}^{(3)}$. Using the coherence matrix for two spatial points $\vec{r}_1$ and $\vec{r}_2$ at time $t$, $W(\vec{r}_1, \vec{r}_2, t) = \left\langle E_i^{(1)}(\vec{r}_1, t) E_j^{(2)*}(\vec{r}_2, t) \right\rangle$, where $i, j = x, z$, which makes us determine the degree of coherence of the field components

$$\eta_{ij}(\vec{r}_1, \vec{r}_2, t) = \frac{W_{ij}(\vec{r}_1, \vec{r}_2, t)}{\sqrt{\mathrm{tr}[W(\vec{r}_1, \vec{r}_1, 0)]}\sqrt{\mathrm{tr}[W(\vec{r}_2, \vec{r}_2, 0)]}} = \frac{W_{ij}(\vec{r}_1, \vec{r}_2, t)}{\sqrt{\sum_{ij} W_{ii}(\vec{r}_1, \vec{r}_1, 0) W_{jj}(\vec{r}_2, \vec{r}_2, 0)}}.$$

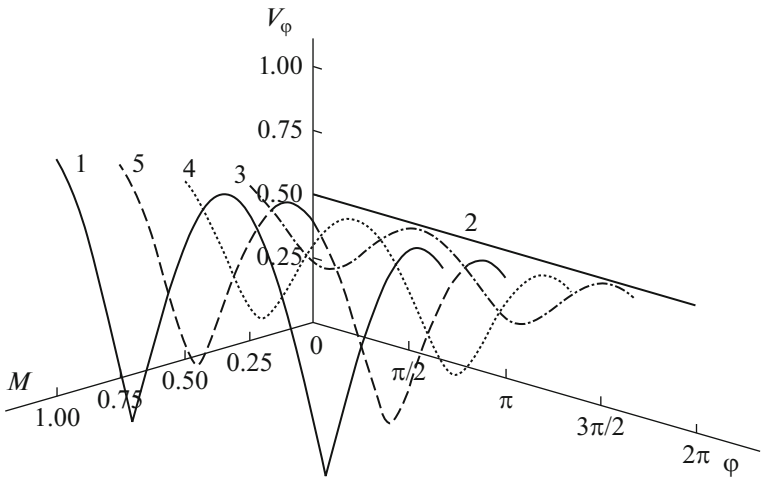


**Fig. 7.** Dependence of the visibility of the interference pattern in the three-beam interference with the change of the reference wave phase φ: curve 1—for the case of absolutely coherence of the initial fields $\eta^{(1,2)} = 1$, VMD corresponds to $M = 1$; curve 2—$\eta^{(1,2)} = 0$, VMD corresponds to $M = 0$; curve 3—$\eta^{(1,2)} = 0.25$, VMD corresponds to $M = 0.25$; curve 4—$\eta^{(1,2)} = 0.5$, VMD corresponds to $M = 0.5$; curve 5—$\eta^{(1,2)} = 0.75$, VMD corresponds to $M = 0.75$.

Then the visibility modulation depth (VMD) is given by

$$M = \max[V^\varphi] - \min[V^\varphi] = 2\sum_m \sum_{ij} \frac{\sqrt{\mathrm{tr}[W(\vec{r}_m, \vec{r}_m, 0]\mathrm{tr}[W(\vec{r}_3, \vec{r}_3, 0)]}}{\varphi_{ij}^{(m)}(\vec{r}) + \varphi_{ij}^{(3)}(\vec{r})} \eta_{ij}^{(m,3)},$$

$m = 1, 2$; $i, j = x, z$. Here $\varphi_{ij}^{(m)}(\vec{r}) = \left\langle E_i^{(m)}(\vec{r}, t) E_j^{*(m)}(\vec{r}, t) \right\rangle$, $m = 1, 2, 3$; $i, j = x, z$.

The physical meaning of the VMD is as follows: we choose a reference wave that is completely correlated with one of the initial waves, for example,$\eta^{(1,3)} = 1$. The phase of the reference wave varies within $0–2\pi$. By selecting the intensity of the three waves, we obtain that the VMD of the interference pattern $M$ corresponds to the degree of mutual coherence between the reference wave and the second of the initial waves, i.e. $M = K\eta^{(2,3)}$, where $K$—is a constant, the value of which depends on the ratio of the corresponding waves' intensity. If $\eta^{(1,3)} = 1$, then $\eta^{(2,3)} = \eta^{(1,2)}$. By an appropriate choice of the intensity of the superposing waves, we can obtain $\eta^{(2,3)} = \eta^{(1,2)}$, then $\eta^{(1,2)}$ will determine the VMD of the interference pattern: $M = \eta^{(1,2)}$, which will make it possible to obtain information on the degree of coherence of the initial beams by measuring the visibility of the resulting distribution (Fig. 7). So, using of the reference wave determines the creation of an optical field in the registration plane, which is modulated in polarization. At the same time, both the spatial polarization modulation and intensity modulation are observed. The last parameter is directly evaluated. Here the role of the third reference wave is diagnostic: in the proposed interference scheme the complex distribution of polarization in the plane of incidence turns into an intensity distribution.

The parameter of VMD has here been introduced. It can also be used for metrology of the degree of coherence of superposing circularly polarized beams of the same direction of rotation of the electrical strength vector with a 90° angle of convergence of the beams. The experimental situation [18, 19, 24], using the condition of preserving the orthogonality of the superposing beams during recording, simulates an optical field in which the spatial polarization modulation is converted into a spatial intensity distribution thus allowing determination of the degree of correlation of the initial optical fields. According to the orientation of the electrical field vector of the reference wave, the visibility of the recorded field changes. A change in the azimuth of the polarization of the reference wave also causes a change in the contrast of the interference pattern. Thus, we can conclude that the polarization component contributes to the field correlation with the possibility of a quantitative assessment of such correlation. Existing approach for reproducing and visualizing of three-dimensional polarization distribution, updating the longitudinal components of the electrical field vector, find their application in systems with ultra-high resolution.

The latest developments of the authors, given in [2], relate to the use of structured light with a three-dimensional polarization distribution for ultra-high spatial resolution systems, while a resolution limit of 10 nm is achieved both in the transverse and longitudinal directions.

## 3. STRUCTURED FIELDS WITH 3D POLARIZATION DISTRIBUTION FOR SUPER RESOLUTION SYSTEMS [2, SEE ALSO THE REFERENCES HEREIN]

In most optical experiments and applications, the polarization in the cross section of the light beam is uniform, or at least close to that. The possibility of obtaining polarized spatially modulated beams in the cross section were understandable, but even before the beginning of the 21'st century they were of no particular interest. This situation changed when radially and azimuthally polarized beams were first realized, which showed extremely intriguing properties with particularly sharp focusing. In the focal region, "needles" of electric and magnetic fields were generated that were oriented along the longitudinal direction of propagation with a beam waist that is smaller than for a standard Gaussian beam. This important result is of interest for applications such as optical nano probes, nanolithography, or for creating high density optical memory. As a rule, the polarization characteristics and distributions of the resulting modes can be easily measured by performing spatially separate Stokes analysis, step by step, in a set of points of the optical field, since the electrical field vector oscillates exclusively in the plane perpendicular to the beam propagation in the paraxial approximation. In the case of light being focused at a level smaller than the wavelength, in order to describe the distribution of the electromagnetic field, it is necessary to take into account its 3D distribution. Due to the appearance of significant transverse wave vectors, one can observe the longitudinal oscillators of the field vector, that is, along the direction of the beam propagation. This phenomenon has powerful prospects for use. To measure individual polarization components in strictly focused fields, separate (individual) fixed-axis fluorescent molecules are used. Subsequently, it was shown that the well-proven near-field tips (probes) used for scanning optical microscopy of the near field can be used to construct a spatial map of the optical fields including the differences between individual polarization components. The spatial phase distribution of the electrical strength components was measured by using a proposed technique due to the study of the obtained interference pattern.

Radially and azimuthally polarized beams are examples of the so-called cylindrical vector beams, i.e. beams that are characterized by a symmetric polarization pattern. These types of beams are related to the wider class of vector beams, in which the linear polarization near the axial optical vortex of the beam, changes azimuthally. Such beams can be used both in optical communication systems and for measuring the mechanical rotational motion of nano- and microparticles. Another type of light beams with a three-dimensional distribution of polarization is the family of Poincare beams, that have all possible polarization states at their intersection and a polarization singularity on the axis. During their propagation, the polarization pattern in the beam changes, that is, in the quantum mode such photons can be described as quantum states with "entangled" polarization, which can be used for some quantum information protocols.

It is in the approximation of three-dimensional polarization structures that it is possible to use all three components of the electromagnetic field, which allows us to generate a field that is structured not only in the transverse plane, but also along the longitudinal coordinate. In this case, the orientation of the polarization ellipse is not limited to the transverse plane, but will change its position in 3D space. This situation could be effectively used for quantum coupling over large distances, even when the influence of turbulence and the magnitude of the beam divergence are significant [2].

More recently, a method for reconstructing a full three-dimensional distributed information, contained in a focused light beam, was presented [25, 26]. This method uses an individual nanoparticle as a device that scans a field. The radiation field, scattered by nanoparticles, can interfere with the incident light beam, used in the study. Information about the local relative phase of the electrical components of the field is embedded in the interference components. This allows us to use the results of measurements of the angular intensity distribution in the far field to restore the amplitude and phase distributions of the focused field.

So, within the framework of this approach, the experimental study of highly complex focal fields with unprecedented resolution becomes absolutely possible. At the same time, there is a need for the development of other methods for studying focal fields with a three-dimensional polarization distribution using the example of the formation of 3D photo images. The development of ultrafast, efficient, and miniature devices that could generate and sort structured beams for metrology applications would be actual. It seems quite understandable that using structured light and its polarization features, it is relatively easy to overcome the classical Rayleigh barrier of transverse resolution. The transition to a three-dimensional distri-

bution of the optical field makes all three components of the electrical strength vector of the waves equal. And the statement that it is likely to achieve a transverse resolution of tens of nanometers seems quite appropriate.

Within this approach, the resolution values are commensurable with similar parameters when estimating the "longitudinal" resolution of optical systems, and this is fully justified in the framework of the 3D (spatial) approach to the optical field structure.

As already noted, nanoscale particles are used to scan complex optical fields, which makes it possible to diagnose the optical field, and will here act as probes of the optical field and allow us to determine the characteristics and parameters of particles that are trapped or transported by internal energy flows.

## 4. GENERAL APPROACHES TO FEMTO-LEVEL MEASUREMENTS

Femto-level measurements are real achievements of present physics, one example of which is the creation and use of femtosecond lasers. Methods that allow converting (transform) laser pulses operating of the auto tuning mode into pulses of almost arbitrary shape were proposed more than two decades ago. Conventional pulse shaping methods use spectral dispersion for spatial separation and subsequent recombination of spectral components, forming a broadband input pulse.

During propagation, the phase and amplitude (sometimes polarization) of individual dispersed optical frequency components can be transformed simultaneously or in parallel by using various modulation technologies. After the frequency components are recombined, the output wavefront will be specified by the inverse Fourier transform of the spatial picture, transferred to the complex optical spectrum. One of the important directions in the formation of femtosecond pulses over the past decade has been associated with the development of optical frequency comb-based lasers, for which the Nobel Prize in Physics was received in 2005 for its tremendous impact on precision frequency metrology and related fields [2, 27, 28]. Such pulse formation approaches are widely used in the technology of ultrafast optical processes. The process of ultrafast wavefront formation is used for coherent laser monitoring of photochemical reactions and quantum mechanical processes, hereunder creating devices for multidimensional optical spectroscopy, for pulse compressing to duration of the visible light oscillation period.

The extremely short pulses, formed at the focus of micro lenses, are used to obtain nonlinear biomedical images for the visualization of micro objects and for laser processing, and for the possibility of unhindered propagation of femtosecond pulses along fibers exceeding 50 km. Another possibility of using femtosecond pulses is to create programmable spatiotemporal fields, which have the property of being focused simultaneously in space and time, deep inside strongly scattering media, such as, for example, in biological tissues.

Another example of femtolevel measurements based on the real results of optical metrology is the use of optical forces of the femto-newton order to manipulate micro- and nano- objects with the study of the feedback effects of objects on optical fields [20, 21, 29–35].

### *4.1. The Use of Micro- and Nanoparticles in Metrology Problems*

A new unique tool that has appeared relatively recently and enables optical metrology to be carried out, is a set of methods for capturing, moving, manipulating, and controlling of the micro- and nanoparticles motion. To this end, optical traps are created in which optical flows can be controlled using a set of field parameters, namely, amplitude, phase, or polarization.

Thus, various types of traps are formed for spatial capture and movement of nanoscale objects, creating active optical forces of the order of femto-newton [31–35].

Comprehensively, considering the methods of creating micro- and nano-manipulators, tweezers and motors, as well as using metrology elements, according to our work [31–37], based on classical optical principles, but supplemented with new, and possibly fundamentally new technical and technological solutions for auxiliary devices, new metrological problems for optical measurements of micro-, nano-, pico-, and femtosecond ranges are solved. Even in the fact that by the speed of microparticles rotation one can determine the absorption coefficient of a matter, the degree of anisotropy of the material, etc. Basically, it can be claimed that these solutions are built on differential, comparative principles and approaches.

### *4.2. Biaxial Crystals in the Tasks of Creating Multifunctional Traps for Micro- and Nano-objects [35]*

Based on modern metrological approaches to achieve a nano (femto) level of optical measurements, the possibility for formation of various amplitude-phase, polarization field structures that can be used for

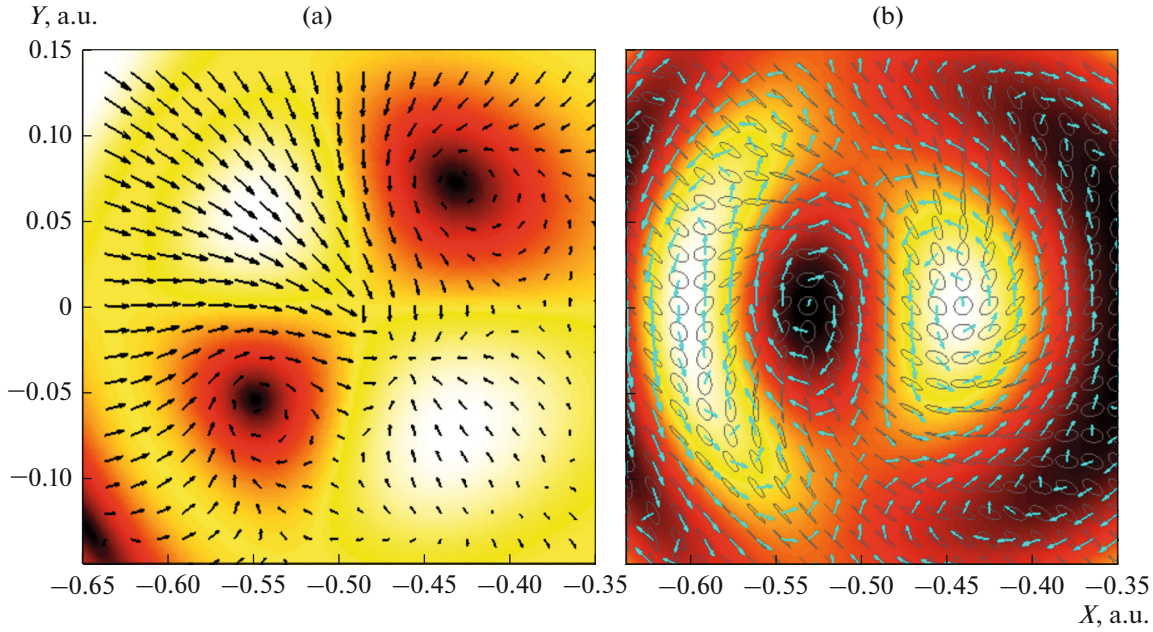


**Fig. 8.** Field distributions at the biaxial crystal output in the vicinity of the optical axis O (both axes lie in the plane (*XZ*) so that $x = 0$ corresponds to the middle direction between the axes); the input beam polarization makes an angle 45° with axis *X*: (a) Intensity distribution after the output *X*-oriented polarizer (background) and the transverse orbital flow of the *X*-polarized component (black arrows); (b) the spin density of the total output field (background), the spin flow map (cyan arrows) and the polarization distribution (gray ellipses).

manipulating micro- and nano-objects is shown in [32–36]. An interesting solution to this problem is that due to the use of birefringent crystals, it is possible to simultaneously work with various parameters of the optical field, creating a wide arsenal of traps based on one crystal.

Created traps, trapping nanoparticle by an optical field provide determination of nanoparticle parameters with high accuracy with an error of several percent [35].

So, the use of birefringent crystals sets the formation optical fields with rich structure of the internal energy flows. Propagation of a slightly divergent (conical) light beam with prescribed linear polarization generates a complicated optical field with spatially inhomogeneous distributions of intensity, phase and polarization that is accompanied by an intricate pattern of the transverse energy flows (Fig. 8).

Such fields offer a variety of possibilities for microparticles' trapping and control, for example:

(a) the intensity minima (maxima) form natural traps for absorbing (dielectric) particles due to the gradient force [39, 40];

(b) phase singularities associated with the amplitude zeros (Fig. 8a) are coupled with the vortex-like orbital flows able to induce rotation of the trapped particle;

(c) both the orbital and spin flows can induce directional motion of particles in the transverse plane (Figs. 8a, 8b);

(d) the spin angular momentum density of the field (Fig. 8b) may induce controllable spinning motion of particles depending on their position within the beam cross section;

(e) the output field pattern can be easily modified via the controllable input and output polarization, which provides suitable means for delicate spatial positioning of the trapped particles.

Arrangement of an optical tweezer employing the above principles is shown in Fig. 9.

On the other hand, as already noted, the use of nano and micro particles provides a diagnostic tool for optical fields. The optical forces arising in the optical field and acting on these particles are at the level of nano-, pico-, femto-Newton, differing in accordance with the properties, shape and size of the particles. Accordingly, it becomes possible to spatially separate internal optical flows, both with respect to spin and orbitally one.

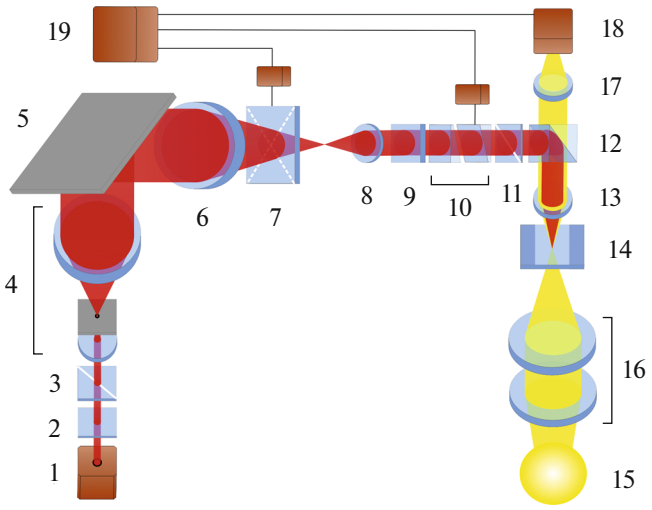


**Fig. 9.** Optical arrangement of tweezers based on a birefringent crystal: (1) laser (650 nm, 200 mW); (2) quarter-wave plate; (3, 11) polarizers; (4) beam expander with spatial filtering; (5) mirror, (6, 8, 13, 17) microobjectives; (7) biaxial crystal with 3D rotating drive; (9) calcite plate; (10) calcite wedges with 2D shifting of one wedge; (12) beam-splitting dichroic cube; (14) sample; (15) white-light source; (16) condenser lenses; (18) CCD-camera; (19) PC.

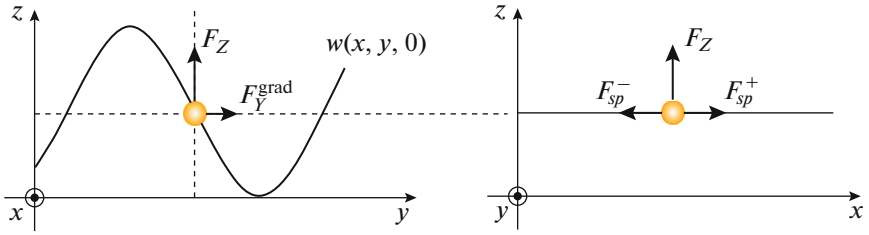


**Fig. 10.** The mechanical action of the incident field on test particles, when including the scattering components, was carried out through the calculation of the Cartesian components of the force ($F_x$, $F_y$, $F_z$) acting on particles that are placed in the optical field. The longitudinal component of the force ($F_z$) represents the traditional action of light pressure, which direct the particles forward; the transverse y-component ($F_y$) corresponds to the gradient force ($F_y^{\text{grad}}$) of an inhomogeneous optical field and traps particles or repels them from areas of high concentration of electromagnetic energy. The most interesting result is the analysis of the component $F_{sp}^{\pm}$ of the optical power along the transverse direction $F_x$—the only component of the force that is associated with the spin flow. This conclusion is confirmed by the fact that, in accordance with the behavior of the spin flow, the value of the force $F_x$ changes its sign with a change of the helicity σ of the incident beam. In the case of linearly polarized light, this component of the force completely disappears [33].

### *4.3. Micro and Nanoparticles as Field Probes*

Our next papers [31–33] demonstrate the results obtained by separating the contribution of the orbital and spin angular momentun to the total picture of trapped particles' motion in the optical field.

To identify the internal spin energy flows [32], it was necessary to analyze the mechanical action of the spin momentum by testing, selecting size and property of the particles. The spin momentum manifests itself "in its pure form" with all the specific properties in the situation of a symmetric superposition of circularly polarized plane waves and thus the formation of a circularly polarized field having inhomogeneous energy (Fig. 10) [31, 33].

Despite the mechanical equivalence of spin and orbital energy flows, that is, their ability to cause translational or orbital motion of the particles under study, the quantitative features of spin-induced and orbital-induced motion, their dependence on the size and properties of the particles are significantly different. That is, the effect of spin and orbital flows can be experimentally distinguished by using test particles with specially selected size and properties. The following figure (Fig. 11) [33] shows the dependence of the components' value of the optical forces on the particle size for different types of particles. The cal-

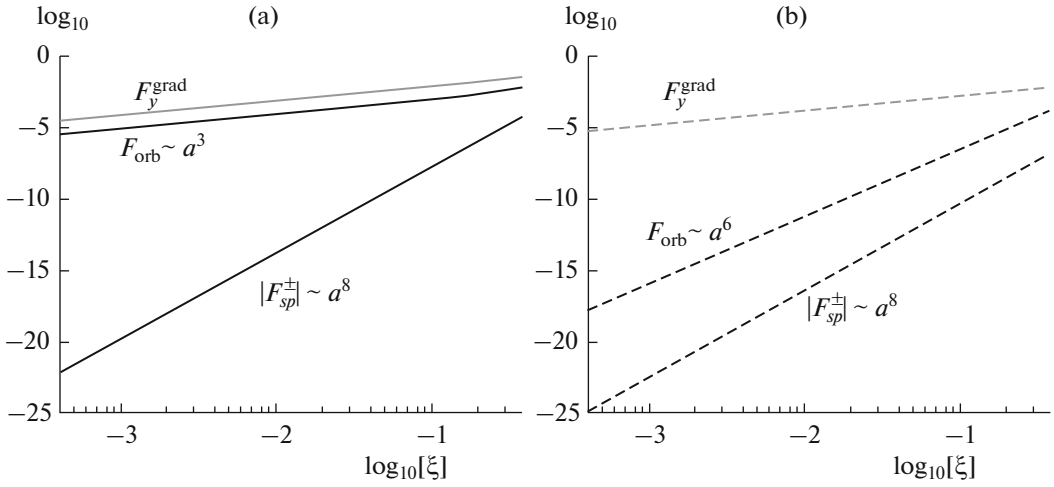


**Fig. 11.** A comparative picture of the mechanical action of the optical forces associated with the spin and orbital internal energy flows is depicted in a double logarithmic scale. The curves are made for particles of small size. Solid lines: metal particles, dotted lines: dielectric particles. The order of optical force growth with a particle radius is indicated taking into account the normalization factor $P_0$. To compare the optical force, the gradient force $F_y^{grad}$ is shown. Here $\xi = ka$ is a dimensionless particle size parameter ($a$—is the particle radius) [33].

culations were performed for two types of spherical particles suspended in water ($\varepsilon = 1.77$, $\mu = 1$, $n = 1.33$): metal (gold hydrosol, relative refractive index $m = 0.32 + 2.65i$ [41]), dielectric (latex in water, $t = 1.12$); wavenumber $k = 1.33 \times 10^5$ cm$^{-1}$ (He-Ne laser).

To eliminate the influence of the incident beam intensity and reduce the number of data presented, the obtained value of the force was normalized by dividing the calculated values by the total momentum of the incident flow over its cross section ($P_0$).

As can be seen from the results of estimating the values of spin and orbital flows shown in the figure, the quantitative features of spin-induced and orbital-induced motions and, accordingly, the generated optical forces, their relationship with the size and properties of the particles are significantly different. Following the main aim of this paper, conducting optical power metrology according to the evaluation results (Fig. 11), we can note the level of optical force up to $10^{-15}$–$10^{-25}$ degree for the spin-induced component of the optical force in accordance with the particle size. We managed to carry out experimental confirmation of the existence of a force of this level in a specially organized experiment [28]. The use of dielectric test particles of the Rayleigh light scattering mechanism made it possible to evaluate experimentally the action of spin and orbital flows. Particles are sensitive to optical forces caused both by spin and orbital flows.

The value of the force is estimated at the level of pico-, femto- Newton, and in accordance with our experiments (Fig. 12) [31] the obtained results can be considered as a proof of the mechanical action of the spin moment (spin energy flow) of the light beam on test particles of the chosen shape and properties. The experimental observation of the polarization-dependent orbital motion of test particles in a transversely inhomogeneous beam with circular polarization, where the rotational action of the orbital momentum density is absent or insignificant, is here demonstrated. Moreover, this demonstration of motion required an ultra-precise experiment, when the peculiarities of the femto- level evaluation of optical force action on nanoparticles is taken into consideration.

In order to observe the action of optical flows on nanoparticles, an optical scheme was chosen in which the lens aperture was selected in order to avoid transforming conversion of spin and orbital flows. Significant numerical apertures do not allow one to study the action of the spin momentum density, since strict focusing of a circularly polarized beam causes a partial transformation of the output spin flow into an orbital one. And even if some mechanical action of the flow is observed, then it is impossible to definitely conclude about the spin or orbital momentum action. To avoid ambiguity, focusing should not be high: the spin-orbital transformation can be neglected (i.e., it does not exceed 1%) when using lenses with a numerical aperture <0.2 (angle $\theta \approx 11°$). Such focusing leads to a certain loss of energy concentration; however, a substantial decrease of the spin action in the focal region can be avoided if the decrease in

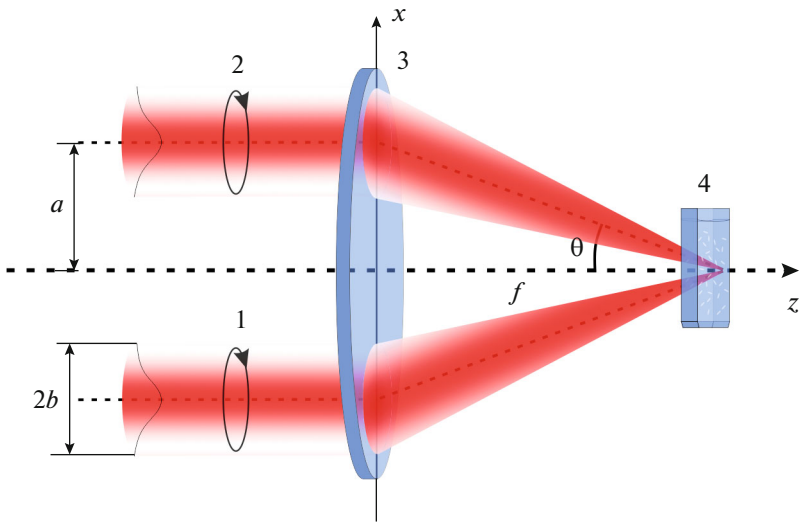


**Fig. 12.** Scheme of the experimental setup: (1), (2) input beams; (3) objective lenses; (4) cuvette with test particles suspended in water.

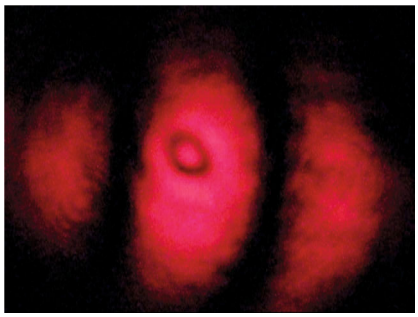

**Fig. 13.** The position of the captured particles within the center of the interference band [31].

intensity is compensated by an increase of the beam inhomogeneity. The above experimental design made it possible to reproduce and record the action of the optical force at the femto level, which is a unique confirmation of the present metrology opportunity. The circulation of energy of a spin nature exists within each band, while the orbital momentum is completely radial and is associated with the beam divergence (Fig. 13) [31]. This radial field momentum can be used to explain the mechanism of particle capture into the desired position outside the center, which allows one to observe the orbital motion associated with the density of the spin momentum.

In an inhomogeneous light field, any dielectric particle is exposed to the action of the gradient force that directs it to the maximum intensity, for example, to the axis of the beam, and vice versa. The radial density of the orbital momentum of the diverging beam creates a value of radial pressure that directs the particle away from the axis. As a result, both forces cancel each other out in certain areas of the interference pattern.

So, by changing the circulation of the electric field vector, the captured particle carries out orbital motion being it clockwise or counterclockwise rotational motion with respect to its own axis. Both the orbital and rotational motions stop when the polarization of the incident beam is linear. The possibility of particle transfer by the force induced by the influence of spin energy flows opens up new prospects for the creation of controlled optical micromachines, micromanipulators in which the regulation and switching are performed through polarization control without changing the beam intensity or its spatial profile. Such methods can be useful in many systems requiring high switching speed.

It should be kept in mind that a nanoparticle is a multifunctional nanoscale tool, playing the role of a separate probe for diagnosing the field structure in the zone of a complex field microdistribution.These nanoparticles are the means of delivering microdoses of drugs into cells, and the unique means of studying

complex macrostructure of the optical field in almost real time. Such a possibility can be realized in water or other transparent solutions with suspended nanoparticles, when the optical force action provides their redistribution into different parts of the complex optical field. New position of these particles could provide information on the spatial distribution of the amplitude, polarization, and, as a result, the phase of the field. There is an expected forecast for the study of speckle fields by nanoparticles, when they are transferred to the points of field singularity by internal energy flows, making it possible to restore information about changes of macro and micro objects over time.

### *4.4. Evanescent Fields for Micro-object Manipulation*

To talk about the influence of an optical field on nanostructures is necessary in order to distinguish the action of evanescent optical fields of a complex energy distribution, in particular in order to transfer microdoses of drugs, providing precise accuracy of the transfer site and the transfer rate of hundreds of nanometers per second [41–43]. This situation becomes possible in the case of excitation of evanescent fields by linearly polarized beams with the azimuth of polarization of 45°. The evanescent field formed in such a way has a special distribution of spin and orbital momentum, i.e. it is elliptically polarized, where the energy circulation is fixed in two planes—a plane parallel to the interface between the two dielectrics, where there is total internal reflection and in the plane perpendicular to it. A specific feature of the excitation of evanescent waves using a linearly polarized wave with azimuth of polarization of 45° is that the transverse spin component, which is responsible for the transverse component of the optical power appears.

In a paper [44], direct measurement of an extraordinary optical momentum and helicity dependent force directed perpendicularly to the wavevector being proportional to the ellipticity of the local polarization of the probing beam has been reported. Such an optical force takes place for evanescent waves and other structured fields being associated with the spin-momentum part of the Poynting vector. The extraordinary transverse momentum has been measured using a femto-newton resolution nano-cantilever immersed in an evanescent optical field above the total internal reflecting glass surface.

In our, later proposed experiments [45, 46], we use a free-standing plate for detection the influence of an evanescent wave. We demonstrate the motion of an optically transparent birefringent microplate influenced by the optical forces arising at the plate plane due to the optical forces caused by simultaneous action of the canonical momentum directed along the wavevector and the transversal spin momentum [47] directed perpendicularly to the canonical momentum, causing the motion in the direction of the Poynting vector, which does not coincide with any of these directions. The surfaces of a birefringent plate have negligible roughness. In order to transfer the transverse momentum to the plate, we deposed gold nanoparticles at its upper surface.

Formation of elliptically polarized wave at a sup-surface layer enables us to estimate the longitudinal and transversal components of the force. Therefore, the vertical spin of an evanescent wave is the source of the last of them.

We simulate the spin and orbital momenta inherent in an evanescent wave when a linearly polarized incidence wave (at upper surface) with the azimuth of polarization 45° reaches the interface plate–air here undergoing TIR. In this case, an evanescent wave that propagates in the z-direction, being damped in the x-direction, can be represented by [44, 47]

$$\vec{E}_{ev} = E\exp(-i\omega t)\left(\vec{x}\frac{1}{\sqrt{1+|m|^2}} + \vec{y}\frac{m}{\sqrt{1+|m|^2}}\frac{k}{k_z} + \vec{z}(-i)\frac{1}{\sqrt{1+|m|^2}}\frac{\kappa}{k_z}\right)\exp(ik_z z - \kappa x),$$

where $k_z = k\frac{n_o}{n}\sin\gamma$, $\kappa = k\sqrt{\left(\frac{n_o}{n}\right)^2\sin^2(\gamma) - 1}$ is the exponential decay rate.

The state of polarization of an evanescent wave [47] is $m = \frac{T_\perp}{T_{//}}m_1$, where $m_1$ is the state of polarization of the probing beam impinging at the interface plate–air being equal to unity for linear polarization with the azimuth of polarization 45°. $\gamma$ is the angle of incidence at the surface, where TIR takes place.

In this case the spin momentum density has both longitudinal and transversal components [47]. Thus, the resulting momentum density in the z-direction possess both orbital and spin momentum density and is given by

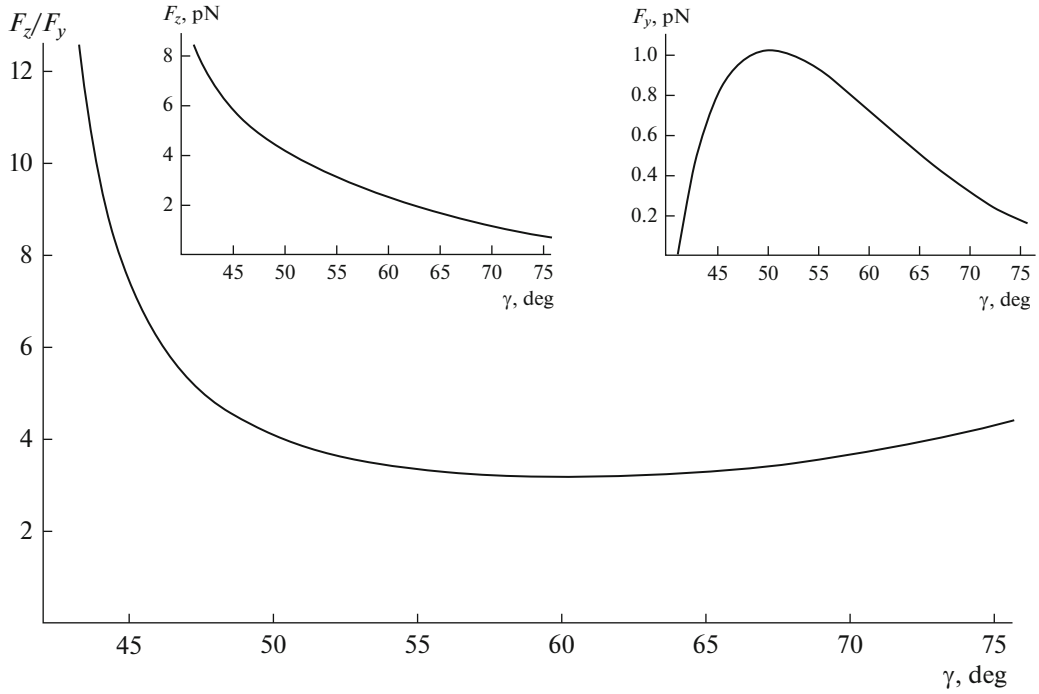


**Fig. 14.** The resulting force in the z-direction ($F_z$), the transverse diagonal polarization-dependent force induced by the vertical spin momentum in the y-direction ($F_y$) and the ratio of optical forces in the longitudinal and transversal directions ($F_z/F_y$) as a function of the incidence angle γ.

$$p_z = p_{oz} + p_{sz} = \frac{A^2}{8\pi\omega}\left[\left(k_z + \frac{m^2k^2}{k_z} + \frac{\kappa^2}{k_z}\right) - 2\frac{\kappa^2}{k_z}\right]\exp(-2\kappa x).$$

The transversal momentum caused by the vertical spin is represented as $p_y = p_{sy} = \frac{A^2}{4\pi\omega}\frac{k\kappa}{k_z}\mathrm{Im}\, m\exp(-2\kappa x)$, where $A = E\frac{1}{\sqrt{1+|m|^2}}$.

Changing the angle of incidence of a beam at the boundary plate-air leads to changing the ellipticity of the evanescent wave excited above the plate surface. That is why one can assume that the magnitude of the transversal spin momentum could be characterized by the different dependence with respect to the resulting momentum in the longitudinal direction, where the main contribution is provided by the canonical momentum. We assume that momentum is transferred by the spherical surface $S$ of the gold particles localized at the plate surface. Light-scattering by particles is taken into account within the Mie approximation [47], giving $\vec{F} = \int_S \Delta\vec{p}\,dS$, where $\Delta\vec{p}$ is the change of momentum density. Simulation of the force affecting a plate and causing its motion presumes integration over the illuminated area assuming a beam aperture 6°. The results of simulation of optical forces induced in the y- and z-directions for a linearly polarized incident beam with the azimuth of polarization 45° versus the incidence angle γ are shown in Fig. 14.

As can be seen from the presented results, the transversal component of the optical force acting from the evanescent field on gold nanoparticles is experimentally fixed in our studies. Experimental study has shown that the motion of the PETF plate depends significantly on the angle of incidence of the beam generating the evanescent wave. The incidence angle affects both velocity and direction of rotation of the plate, as well as the angle of deviation of the forward movement from the z-axis.

In our experiment [45, 46] one observes simultaneous plate rotation and forward movement. The rotation of the plate stops, when the main optical axis of the plate coincides with the azimuth of polarization of the incident beam, continuing the rectilinear motion until the plate leaves the beam. Rotation vanishes precisely for linearly polarized wave impinging onto the upper surface of a plate at an angle ±45°, due to the birefringence torques being compensated. This is achieved for an angle of incidence of the probing

beam about 58°, which gives the azimuth of polarization of this beam at bottom interface equal to 62°. Therefore, rectilinear motion of the plate without rotation is possible due to the action of the transversal component of the optical force generated above the plate. The angle between the motion direction and z-axis is 15°.

The use of these effects for evanescent waves [48, 49], in particular, is relevant for the development of nanotechnology, including molecular, especially for biomedicine, nano-therapy, transportation of medical products, bio-marking, cancer diagnosis, and bio-probing. All this provide a new tool to investigate cell properties, i.e. mechanical or optical parameters and charachteristics [49].

This brings about non-invasive methods for evaluating and analyzing pathological changes in tissues with the search for new opportunities for treating diseases and possible pathologies by non-traumatic, easily accessible methods.

### *4.5. Metrology of Optical Parameters for Low-absorbing Microparticles*

The next step of our paper is to demonstrate one of the metrological solutions for determining the absorption coefficient of low-absorbing microparticles by estimating the rotation speed of such objects in the field of a circularly polarized beam [50]. The uniqueness of the proposed experimental approach is that the accuracy in determining the optical parameter is of the order of femto units. It is a confirmation of the breakthrough in optical metrology and relies on the fact that modern experimental equipment and corresponding experimental approaches and measurements have lifted the microrange up to a new, more delicate level.

In particular, we present results obtained by studying the microscopic properties of liquids and various biological samples by complex optical fields [51, 52]. The optical field, acting on particles, transfers part of the momentum to them, thereby causing the spatial motion of the particles. The characteristics of this motion substantially depend on the optical constants of the studied micro- and nanoparticles.

Even the properties of complex solid samples containing, as impurities, various kinds of inclusions in the form of a fine-grained structure are determined by the optical properties of these micro and nanoparticles, thereby opening for applications. A change of the radiation propagation conditions substantially depends on the attenuation of the radiation, here determined by the absorption and scattering of radiation on these structures.

Traditionally, solutions to such problems are sought through using of Mie scattering theory, which allows one to determine mechanical ponderomotive factors (force and torque) which an optical field exerts on a particle. More importantly, the ponderomotive factors can be directly associated with the optical parameters of the particle, and this can be employed for their measurement.

In [50], the criterion of optical fields action on micro- and nano-particles is the rotational motion of the particle under the influence of a torque, which is inherent in an optical field of circular polarization with a spin angular momentum.The spinning motion of the particle is due to the field spin angular momentum absorbed by the particle, and its angular velocity $\Omega$ is related to the radiation torque by the equation

$$\Omega = \frac{T}{8\pi\eta r^3},$$

where $\eta = 8.9 \times 10^{-3}$ dyn s cm$^{-2}$ (at 25°C) is the dynamical viscosity of the medium. $T$ is an absolute torque, which is calculated through Mie theory $T = 4\pi I \frac{n}{\varepsilon c}\sigma\left(\mathrm{Im}\left(\alpha_e\right) - \frac{2k^3}{3\varepsilon}|\alpha_e|^2\right)$, here $\alpha_e$—is the polarizability, appears due to the particle absorption. $I$ is the energy flow density in the wave, $c$ is the light velocity in vacuum, $\omega$ is the wave frequency, $k = (\omega/c)n$ is its wavenumber, and $\sigma$ is the wave spin number equal to $\pm 1$ for right (left) circular polarization, respectively, and 0 for any linear or no polarization. Here the particle is assumed to be immersed in a homogeneous isotropic dielectric medium with real permittivity $\varepsilon$ and real permeability $\mu$ so that the refraction index equals to $n = \sqrt{\varepsilon\mu}$.

The absorption index $\kappa$ of the particle suspended in water and trapped in the center of a focused Gaussian beam waist with radius $w_0 = 2$ μm can be directly derived from the observed spinning velocity $\Omega$ exhibited by the particle in the beam with power $P = 100$ mW, $\kappa = q\frac{\Omega}{P}$, where $q$ is the transition coefficient. At the same time, the particle must have low absorption, so that there is no local heating of the medium sur-

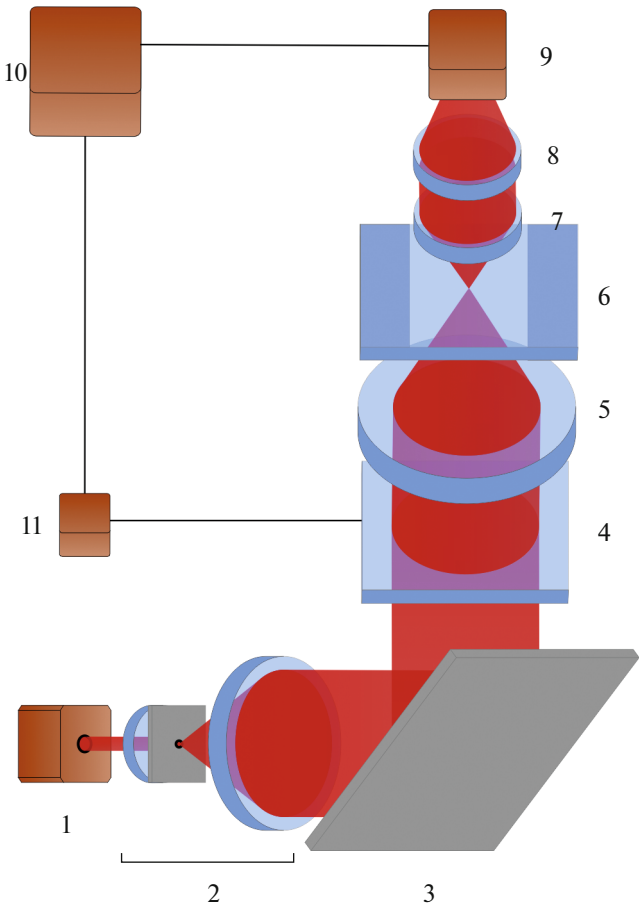


**Fig. 15.** Schematic of the experimental setup: (1) laser; (2) beam expander with spatial filter; (3) mirror; (4) quarter-wave plate; (5), (7) and (8) objective lenses; (6) cell with probing particles suspended in water; (9) CCD-camera; (10) personal computer; (11) control unit.

rounding the particle. Effective particle capture requires that the particle size be several times smaller than the size of the focused spot, but in such a way as to prevent diffraction by the captured object.

We have used weakly absorbing ($\kappa \le 10^{-3}$) dielectric particles with diameter 0.5 to 2 μm. A schematic of the experimental equipment [50] is presented in the following Fig. 15.

As a result of the optical field action, the particle acquires a rotational motion, and the angular velocity of the particle corresponds to the part of the torque that is absorbed. As absorption increases, an acceleration of the rotational motion is observed. The measured value of the spinning velocity obtained in the experiment, e.g. for a gamboge particle of about $\Omega_e = 25.8\ s^{-1}$, differs from the theoretically obtained spinning velocity and amounts to about 20%. Such an error can be explained by the longitudinal displacements of the particle with respect to the beam waist, heating of the cell with particles, changes in the properties of water inside the cell, and other reasons. The introduction of the normalization coefficient, obtained by comparing the theoretical and experimental results, made it possible to determine the value of the particle absorption coefficient, here for this type of particle, giving $12.4 \times 10^{-4}$.

Of course, the question arises about the accuracy of the proposed method for measuring the absorption index. The flexibility of this method is determined by the refractive properties of the particle, the density of the medium where the particles are dispersed, the characteristics of the irradiating beam, and the cross-section of the focused beam. Restrictions for the determination of the particle rotation speed of about $0.1 s^{-1}$ are formed. Then, with the introduction of transition coefficient ($q$), the error in estimating the absorption coefficient $\delta$ can be obtained in the range $10^{-8} \le \delta \le 4 \times 10^{-7}$. Obtaining reliable results of measuring the absorption coefficient of particles is possible for absorption less than $10^{-2}$.

Thus, the possibility of directly assessing the value of the index of light absorption by microparticles became possible thanks to the proposed approach, which uses the principles of capture and rotation of microparticles by internal energy flows. The current state of the development of technology for the manipulation of microobjects of various nature and properties makes the proposed method of metrology of optical properties encouraging and promising for many practical applications. The obtained results are the first step in solving this kind of metrological problems. The high sensitivity of the absorption index metrology, the high accuracy of the estimation of the measured parameter, upon reaching the appropriate level of control for the measurement conditions, makes it possible to use this method to study weakly absorbing particles.

The above-mentioned results on the involvement of the technique of micro and nanoparticles in the study of complex optical fields, the transition to control of the particle movement within a few angstroms with the acting force on the captured object at the level of femto Newton have opened the new possibilities of modern metrology. Such approaches are already used today to manipulate organelles in cells, to study viscoelastic properties, to build molecular motors and will find their implementation among many other interesting applications.

## 4. OPTICAL METROLOGY OF ROUGH SURFACES

The next step in presenting the results of research and development on the latest methods of optical metrology is diagnostic methods for processing extremely smooth surfaces with ultra-high precision accuracy [53, 54].

Two techniques for measuring of roughness, based on measurement of the phase variance of the boundary object field and on a transverse coherence function of a field, as well as the devices implementing these techniques were proposed in our papers [53, 54]. The following principles form the base of the proposed techniques:

• heights of surface microirregularities are less than the wavelength of the probing radiation, ($R_q < 0.1$ mm), and the transversal scale of surface irregularities is larger than the wavelength, so that the specular component of the reflected radiation is present;

• phase variance is measured at the boundary field (the sample surface is imaged at the plane of analysis); the transversal coherence function of a field can be measured at arbitrary zone;

• statistical parameters of a field are measured with interferometric means, within the zero (infinitely extended) interference fringe.

The first technique (Fig. 16) is used for measuring of surface roughness based on measurement of a phase variance of the boundary object field [55–58].

Using an interrelation between the height parameters of surface roughness and the phase parameters of the boundary object field, one obtains the following equation for a root mean square deviation (RMS) roughness:

$$RMS = \frac{\lambda}{4\pi}\sqrt{\frac{I(x,y)}{I_o}}.$$

Technical parameters of the device are the measured RMS range—0.002 to 0.08 μm, the measurement accuracy—0.001 μm, the measurement scheme—micro-interferometer, indication rate—one measurement per five second, indicated units—micrometers. Here $\langle I(x,y)\rangle, I_0$ are the resulting field and the object beam intensity, respectively.

This device could be used for measuring the plane and spherical surfaces with a radius of curvature larger than 0.2 m in polishing machine tool for surface quality control during making of details. This device can be made as a stationary instrument.

The second one is a technique for measuring of surface roughness based on measurement of a field's transverse coherence function (Fig. 17) [54].

Another method for measuring the phase variance utilizes the relationship between the transverse coherence function $\Gamma_\perp(\rho)$ of the scattered field, on the one hand, and the statistical parameters of the object, on the other hand. The RMS height deviation can be found from the relation $\mathrm{RMS} = \frac{\lambda}{4\pi}\sqrt{-\ln\frac{I_{\max} - I_{\min}}{I_{\max} + I_{\min}}}$, $I_{\max}$ and $I_{\min}$ are the maximum and minimum resulting intensity, respectively. The information contained in the resulting interference pattern is extracted by transforming the optical signal into electric ones with subsequent processing in the analogue electronic unit CU.

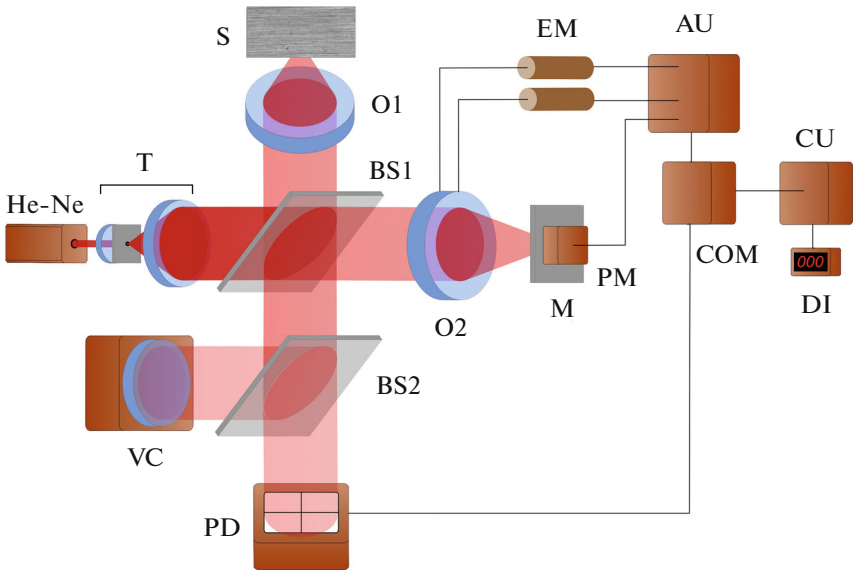


**Fig. 16.** Experimental arrangement for measuring the degree of low-reflectance surface roughness: He-Ne—laser, T—telescope, BS1, BS2- beam-splitters, O1,O2—objective lenses, S—sample, M—mirror, PM—piezo-ceramic modulator, PD—2 × 2 position-sensitive photodetector array, VC—visualization channel, EM—electric motors, AU—automatic zero fringe adjustment unit, COM—comparator, CU—analogue $R_q$ calculation unit, DI—digital indicator.

Two versions of the device for surface roughness control based on measuring of the field's transverse coherence function were displayed:

—A stationary device that can be mounted on the processing tool. Device intended for measuring the RMS height deviations of slightly rough surfaces over the range from 0.002 μm to 0.06 μm. Technical parameters are measured RMS range—0.003 to 0.10 μm, measurement accuracy—0.002 μm. Update rate—one measurement per second. Fields of application are the following: arbitrarily shaped surfaces with a radius of curvature larger than 0.3 m; the photochemical industry to monitor the quality of calendar shafts; space industry to monitor the quality of mirrors fabricated by diamond micro-sharpening; polishing machine tool. This device was used for surface quality on-line control.

—Portable device for control of large-area or small-area surfaces. Portable device intended for measuring the RMS height deviations of slightly rough surfaces. Main technical parameters of the device are the measured RMS range—0.005 to 0.10 μm, the measurement accuracy—0.002 μm, the update rate—one measurement per second. This device provides the following field of application: polishing machine tool, this device was used for the surface quality control during making of details; device can be made either as a measuring head, or as a stationary instrument, depending on the size and the position of the object to be controlled.

Sensitivity of the RMS height parameter of all these devices down to 10 Å was achieved. Roughness control of slightly rough (polished) surfaces with RMS deviation of a profile from a mean surface line ranging from 0.002 μm to 0.10 μm. The technique is applicable to metallic, insulator, semiconductor, and optical surfaces.

## 5. OPTICAL REFRACTIVE INDEX METROLOGY

Finally, we would like to bring forward one more aspect of fine metrological measurement related to the determination the refractive index of a light-scattering liquid media. Here, a specific issue is polarization interferometry to find the refractive index of solutions, suspensions and gaseous media [59]. According to the proposed approach [60], a two-beam interferometer is used to determine the refractive index, in which a circularly polarized beam is formed in each channel. The measurement method consists in splitting the optical radiation into two components and forming mutually orthogonal circular polarizations of the field components. As a result of superposition of such beams, a uniform intensity distribution is seen in the interference plane. In this case, the formed field has some deterministic polarization. The resulting field is linearly polarized and is characterized by the azimuth of polarization $\alpha_0$, when the studied solution is located in the object channel giving rise to polarization change of the transmitted radiation.

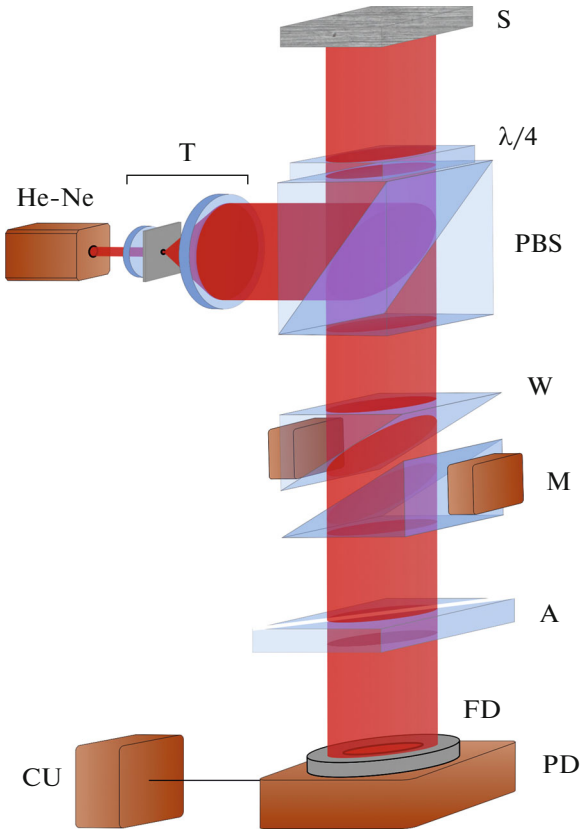


**Fig. 17.** Experimental arrangement for measuring the degree of arbitrary surface roughness: He–Ne—laser, T—telescope, PBS—polarizing beamsplitter, S—sample, W—calcite wedges; M—electromechanical modulator, A—analyzer; FD—field-of-view diaphragm; PD—photodetector, CU—analogue $R_q$ calculation unit.

As a result, a rotation of the azimuth of linear polarization is observed in the interference plane, which takes on the value $\alpha$. Thus the difference in polarization azimuth is $\alpha - \alpha_0$, which is related to the reduced path difference of the beams in the arms of the interferometer, given by $n = n_0 + \Delta n_0 = n_0 + \dfrac{(\alpha - \alpha_0)\lambda}{2\pi l_0}$, where $n_0$ is the refractive index of the main medium (solvent), and $l_0$ is the cell thickness.

The azimuth of polarization of the resulting distribution is sensitive to variations in the path difference in the arms of the interferometer. Even with a change in the path difference between the orthogonal components by an amount less than $\lambda$, the polarization azimuth will change significantly. If the path difference between the orthogonal components is $\lambda$, then the polarization azimuth will change by $2\pi$. The polarization azimuth can be measured with an accuracy of some seconds. As a result, the accuracy of path difference measuring ($\Delta l$) is $10^{-5}\lambda$, and the accuracy of measuring the value of the refractive index is $10^{-6}\dfrac{\lambda}{l_0}$.

## CONCLUSIONS

The results presented in this paper provide an overview of the metrological approaches and results obtained by the authors of this paper and specialists in the field of optical metrology over the past decades, in the direction of ultra-sensitive precision measurements. The level of sensitivity of the methods achieved by interference, polarization-interference when assessing the roughness of smooth surfaces, when measuring variations in the refractive index of aqueous solutions; when evaluating phase shifts as a result of total internal reflection of orthogonally linearly polarized field components, etc. ranges from tens of angstroms to tens of nanometers. Such approaches are embedded in the existing interconection between the correlation and polarization parameters of optical fields in various model situations of beams' superposition. The deepening of approaches for the determination the degree of the beam correlation that is con-

tained in the theory of coherence, the enrichment of these approaches, cause the expansion of the optical metrology base through the involvement of fine interference methods in modern optics. The results obtained when searching for ways to achieve femto- and picosecond light pulses are in good agreement with the given estimates. According to the latest new results on the use of structured light in the problems of creating systems with super-resolution within the framework of three-dimensional polarization distribution approaches with increased importance of the longitudinal component allows the users to overcome the classical transverse resolution barrier and reach the limit of tens of nanometers.

The femto level of optical forces, which occurs in complex optical fields with a rich morphology of the distribution of internal optical energy flows, interacts with micro- and nano-objects of various shapes and properties, but also control their spatial motion in optical traps, the nature of which can differ significantly in accordance with the trap formation mechanism. The optical forces of this physical nature and the values are used to determine the optical parameters of trapped particles, where the accuracy of the determination is controlled at the nanoscale level.

The nature of the trap is different, but the original and novelty of our approaches are the use of biaxial crystals, which allowed us to form a complex distribution of internal energy flows and at the same time realize the conversion from phase-amplitude to polarization structures intended for nano-objects capture. It is clear that this review cannot be a complete analysis of new modern ultra fine methods of optical metrology. It is also worth recalling the ideas and principles of STED microscopy [61–63], the physical principles of the operation of optical vortex coronographs [64], and much more. As an modern optical metrology feature it could be noted the fundamentally achievable opportunity to operate and manipulate with atoms [2]—this is the ultimate fantasy for the optical range.

## CONFLICT OF INTEREST

The authors declare that they have no conflicts of interest.

## REFERENCES

1. Hell, S.W., Nanoscopy with focused light (Nobel Lecture), *Angew. Chem., Int. Ed. Rev.,* 2015, vol. 54, pp. 8054–8066.
2. Rubinsztein-Dunlop, H. et al., Roadmap on structured light, *J. Opt.,* 2017, vol. 19, p. 013001.
3. Rotenberg, N. and Kuipers, L., Mapping nanoscale lightfields, *Nat. Photonics,* 2014, vol. 9, p. 919.
4. Bauer, T. et al., Observation of optical polarization Möbius strips, *Science,* 2015, vol. 347, p. 964.
5. Geng, J., Structured-light 3D surface imaging: a tutorial, *Adv. Opt. Photonics,* 2011, vol. 3, pp. 128–133.
6. Bliokh, K.Y. and Aiello, A., Goos–Hänchen and Imbert–Fedorov beam shifts: an overview, *J. Opt.,* 2013, vol. 15, no. 1, p. 014001.
7. Aiello, A., Goos–Hänchen and Imbert–Fedorov shifts: a novel perspective, *New J. Phys.*, 2012, vol. 14, p. 013058.
8. Zoghi, M., Goos–Hänchen and Imbert–Fedorov shifts in a two-dimensional array of gold nanoparticles, *J. Nanophotonics,* 2018, vol. 12, no. 1, p. 016021.
9. Goswami, S., Dhara, S., Pal, M., Nandi, A., Panigrahi, P.K., and Ghosh, N., Optimized weak measurements of Goos–Hänchen and Imbert–Fedorov shifts in partial reflection, *Opt. Express,* 2016, vol. 24, no. 6, pp. 6041–6051.
10. Hosten, O. and Kwiat, P., Observation of the spin Hall effect of light via weak measurements, *Science,* 2008, vol. 319, no. 5864, pp. 787–790.
11. Tervo, J., Coherence and polarization in stationary random electromagnetic fields, *Opt. Pura Appl.,* 2005, vol. 28, no. 3, pp. 27–36.
12. Tervo, J., Setäla, T., and Friberg, A.T., Degree of coherence for electromagnetic fields, *Opt. Express,* 2003, vol. 11, pp. 1137–1143.
13. Réfrégier, Ph. and Goudail, F., Invariant degrees of coherence of partially polarized light, *Opt. Express,* 2005, vol. 13, no. 16, pp. 6051–6060.
14. Setälä, T., Tervo, J., and Friberg, A.T., Contrasts of Stokes parameters in Young's interference experiment and electromagnetic degree of coherence, *Opt. Lett.,* 2006, vol. 31, no. 18, pp. 2669–2671.
15. Refregier, P. and Roueff, A., *Intrinsic Coherence: A New Concept in Polarization and Coherence Theory,* OPN, 2007, pp. 30–35.
16. Wolf, E., Unified theory of coherence and polarization of random electromagnetic beams, *Phys. Lett. A,* 2003, vol. 312, pp. 263–267.
17. Ellis, J., and Dogariu, A., Complex degree of mutual polarization, *Opt. Lett.,* 2004, vol. 29, no. 6, pp. 536–538.

18. Angelsky, O.V., Hanson, S.G., Zenkova, C.Yu., Gorsky, M.P., and Gorodyns'ka, N.V., On polarization metrology (estimation) of the degree of coherence of optical waves, *Opt. Express,* 2009, vol. 17, no. 18, pp. 15623–15634.

19. Angelsky, O.V., Zenkova, C.Yu., Gorsky, M.P., and Gorodyns'ka, N.V., On the feasibility for estimatingthe degree of coherence of waves at near field, *Appl. Opt.,* 2009, vol. 48, vol. 15, pp. 2784–2788.

20. Angelsky, O.V., Gorsky, M.P., Maksimyak, P.P., Maksimyak, A.P., Hanson, S.G., and Zenkova, C.Yu., Investigation of optical currents in coherent and partially coherent vector fields, *Opt. Express,* 2011, vol. 19, no. 2, pp. 660–672.

21. Zenkova, C.Yu., Gorsky, M.P., Maksimyak, P.P., and Maksimyak, A.P., Optical currents in vector fields, *Appl. Opt.,* 2011, vol. 50, no. 8, pp. 105–1112.

22. Angelsky, O.V., Polyanskii, P.V., Mokhun, I.I., Zenkova, C.Yu., Bogatyryova, H.V., Felde, Ch.V., Bachinskiy, V.T., Boichuk, T.M., and Ushenko, A.G., *Optical Measurements: Polarization and Coherence of Light Fields, Modern Metrology Concerns*, Cocco, L., Ed., InTech, 2012.

23. Zenkova, C.Yu., Gorsky, M.P., and Gorodynska, N.V., Metrology of degree of coherence of circularly polarized optical waves, *Opto-Electron. Rev.,* 2011, vol. 19, no. 3, pp. 14–19.

24. Zenkova, C.Yu., Yermolenko, S.B., Angelskaya, A.O., and Soltys, I.V., The polarization peculiarities of the correlation (intrinsic coherence) of optical fields, *Opt. Mem. Neural Networks,* 2011, vol. 20, no. 4, pp. 247–254.

25. Bauer, T., Orlov, S., Peschel, U., Banzer, P., and Leuchs, G., Nanointerferometric amplitude and phase reconstruction oftightly focused vector beams, *Nat. Photonics,* 2014, vol. 8, no. 23.

26. Novotny, L., Beversluis, M.R., Youngworth, K.S., and Brown, T.G., Longitudinal field modes probed by singlemolecules, *Phys. Rev. Lett.,* 2001, vol. 86, no. 23, pp. 5251–5254.

27. Ye, J. and Cundiff, S.T., *Femtosecond Optical Frequency, Comb Technology*, New York: Springer, 2005.

28. Schimpf, D.N., Olgun, H.T., Kalaydzhyan, A., Hua, Y., Matlis, N.H., and Kärtner, F.X., Frequency-comb-based laser system producing stable optical beat pulses with picosecond durations suitable for high-precision multi-cycle terahertz-wave generation and rapid detection, *Opt. Express,* 2019, vol. 27, no. 8, pp. 11037–11056.

29. Zenkova, C.Yu., Gorsky, M.P., Soltys, I.V., and Angelsky, P.O., The investigation of the peculiarities of the motion of testing nanoobjects in the inhomogeneously-polarized optical field, *Opt. Mem. Neural Networks,* 2012, vol. 21, no. 1, pp. 34–44.

30. Zenkova, C.Yu., Gorsky, M.P., Soltys, I.V., and Angelsky, P.O., On the possibilities of using inhomogeneity in light energy distribution for estimating the degree of coherence of superposing waves, *Appl. Opt.,* 2012, vol. 51, no. 10, pp. C38–C43.

31. Angelsky, O.V., Bekshaev, A.Ya., Maksimyak, P.P., Maksimyak, A.P., Hanson, S.G., and Zenkova, C.Yu., Orbital rotation without orbital angular momentum: mechanical action of the spin part of the internal energy flow in light beams, *Opt. Express,* 2012, vol. 20, no. 4, pp. 3563–3571.

32. Angelsky, O.V., Bekshaev, A.A., Maksimyak, P.P., Maksimyak, A.P., Mokhun, I.I., Hanson, S.G., Zenkova, C.Yu., and Tyurin, A.V., Circular motion of particles suspended in a Gaussian beam with circular polarization validates the spin part of the internal energy flow, *Opt. Express,* 2012, vol. 20, no. 10, pp. 11351–11356.

33. Bekshaev, A.Ya., Angelsky, O.V., Hanson, S.G., and Zenkova, C.Yu., Scattering of inhomogeneous circularly polarized optical field and mechanical manifestation of the internal energy flows, *Phys. Rev. A,* 2012, vol. 86, no. 2, p. 023847.

34. Zenkova, C., Soltys, I., and Angelsky, P., The use of motion peculiarities of particles of the Rayleigh light scattering mechanism for defining the coherence properties of optical fields, *Opt. Appl.,* 2013, vol. 43, no. 2, pp. 297–312.

35. Berry, M.V., Optical currents, *J. Opt. A: Pure Appl. Opt.,* 2009, vol. 11, p. 094001.

36. Angelsky, O.V., Bekshaev, A.Ya., Maksimyak, P.P., and Polyanskii, P.V., Internal energy flows and optical trapping, *Opt. Photonics News,* 2014, vol. 25, no. 12, pp. 20–21.

37. Ushenko, A.G., Ermolenko, S.B., Burkovets, D.N., and Ushenko, Y.A., Polarization microstructure of laser radiation scattered by optically active biotissues, *Opt. Spectrosc.,* 1999, vol. 87, pp. 434–438.

38. Angelsky, O.V., Bekshaev, A.Ya., Maksimyak, P.P., Maksimyak, A.P., Hanson, S.G., and Zenkova, C.Yu., Self-diffraction of continuous laser radiation in a disperse medium with absorbing particles, *Opt. Express,* 2013, vol. 21, no. 7, pp. 8922–8938.

39. Dienerowitz, M., Mazilu, M., and Dholakia, K., Optical manipulation of nanoparticles: a review, *J. Nanophotonics.* 2008, vol. 2, p. 021875.

40. Bekshaev, A.Ya., Subwavelength particles in an inhomogeneous light field: Optical forces associated with the spin and orbital energy flows, *J. Opt.,* 2013, vol. 15, p. 044004.

41. Angelsky, O.V., Maksymyak, P.P., Zenkova, C.Yu., Maksymyak, A.P., Hanson, S.G., and Ivanskyi, D.I., Peculiarities of control of erythrocytes moving in an evanescent field, *J. Biomed. Opt.,* 2019, vol. 24, no. 5, p. 055002.

42. Angelsky, O.V., Zenkova, C.Yu., and Ivanskyi, D.I., Mechanical action of the transverse spin momentum of an evanescent wave on gold nanoparticles in biological objects media, *J. Optoelectron. Adv. Mater.,* 2018, vol. 20, no. 5–6, pp. 217–226.

43. Angelsky, O.V., Zenkova, C.Y., Maksymyak, P.P., Maksymyak, A.P., Ivanskyi, D.I., and Tkachuk, V.M., Peculiarities of energy circulation in evanescent field. Application for red blood cells, *Opt. Mem. Neural Networks,* 2019, vol. 28, no. 1, pp. 11–20.

44. Antognozzi, M., Bermingham, C.R., Hoerber, H., Dennis, M.R., Bekshaev, A.Ya., Harniman, R.L., Simpson, S., Senior, J., Bliokh, K.Y., and Nori, F., Direct measurements of the extraordinary optical momentum and transverse spin-dependent force using a nano-cantilever, *Nat. Phys.,* 2016, vol. 12, pp. 731–735.

45. Angelsky, O.V., Hanson, S.G., Maksimyak, P.P., Maksimyak, A.P., Zenkova, C.Yu., Polyanskii, P.V., and Ivanskyi, D.I., Influence of evanescent wave on birefringent microplates, *Opt. Express,* 2017, vol. 25, no. 3, p. 2299.

46. Zenkova, C.Yu., Ivanskyi, D.I., and Kiyashchuk, T.V., Optical torques and forces in birefringent microplate, *Opt. Appl.,* 2017, vol. 47, no. 3, pp. 483–493.

47. Bliokh, K.Y., Bekshaev, A.Y., and Nori, F., Extraordinary momentum and spin in evanescent waves, *Nat. Commun.,* 2014, vol. 5.

48. Yoon, Y.-Z. and Cicuta, P., Optical trapping of colloidal particles and cells by focused evanescent fields using conical lenses, *Opt. Express,* 2010, vol. 18, no. 7, p. 7076.

49. Gu, M., Kuriakose, S., and Gan, X., A single beam near-field laser trap for optical stretching, folding and rotation of erythrocytes, *Opt. Express,* 2007, vol. 15, no. 3, p. 1369.

50. Angelsky, O.V., Bekshaev, A.Ya., Maksimyak, P.P., Maksimyak, A.P., and Hanson, S.G., Measurement of small light absorption in microparticles by means of optically induced rotation, *Opt. Express,* 2015, vol. 23, no. 6, pp. 7152–7163.

51. Bishop, A.I., Nieminen, T.A., Heckenberg, N.R., and Rubinsztein-Dunlop, H., Optical application and measurement of torque on microparticles of isotropic nonabsorbing material, *Phys. Rev. A,* 2003, vol. 68, no. 3, p. 033802.

52. Svoboda, K. and Block, S.M., Biological applications of optical forces, *Annu. Rev. Biophys. Biomol. Struct.,* 1994, vol. 23, no. 1, pp. 247–285.

53. Angelsky, O.V., Maksimyak, P.P., and Hanson, S., *The Use of Optical-Correlation Techniques for Characterizing Scattering Object and Media*, Bellingham, USA: SPIE Press PM71, 1999.

54. Angelsky, O.V. and Maksimyak, P.P., Optical Correlation Diagnostics of Surface Roughness, in *Optical Correlation Applications and Techniques*, Bellingham, USA: SPIE Press, 2007.

55. Angelsky, O.V. and Maksimyak, P.P., *Optical correlation diagnostics of surface roughness in coherent-domain optical methods, Biomedical Diagnostics Environmental and Material Science*, Tuchin, V.V., Ed., Kluwer Academic Publ., 2004, Chap. 2.

56. Angelsky, O.V., Ushenko, A.G., Pishak, V.P., Pishak, O.V., and Ushenko, Yu.A., Coherent introscopy of phase-inhomogeneous surfaces and layers, *Proc. SPIE*, 2000, vol. 4016, pp. 413–418.

57. Angel'skii, O.V., Ushenko, O.G., Burkovets, D.N., Arkhelyuk, O.D., and Ushenko Y.A., Polarization-correlation studies of multifractal structures in biotissues and diagnostics of their pathologic changes, *Laser Phys.*, 2000, vol. 10, no. 5, pp. 1136–1142.

58. Angelsky, O.V. and Maksimyak, P.P., Optical diagnostics of slightly rough surfaces, *Appl. Opt.*, 1992, vol. 31, no. 1, pp. 140–143.

59. Nagibina, I.N., *Interefeance and Diffraction of Light*, Mashynostroenie, 1985 (in Russian).

60. Angelsky, O.V., Maksymyak, P.P., and Polyansky, V.K., *Measuremeny of refractive index of light scattering media*, Avtorskoye svidetelstvo, 1986 (in Russian).

61. Punge, A., Rizzoli, S.O., Jahn, R., Wildanger, J.D., Meyer, L., Schonle, A., Kastrup, L., and Hell, S.W., 3D reconstruction of high-resolution STED microscope images, *Microsc. Res. Tech.,* 2008, vol. 71, pp. 644–650.

62. Westphal, V. and Hell, S.W., Nanoscale resolution in the focal plane of an optical microscope, *Phys. Rev. Lett.,* 2005, vol. 94, pp. 143903–143904.

63. Vicidomini, G., Bianchini, P., and Diaspro, A., STED super-resolved microscopy, *Nat. Methods,* 2018, vol. 15, pp. 173–182.

64. Valle, P.J., Fuentes, A., Canales, V.F., Cagigas, M.A., Villo-Perez, I., and Cagigal, M.P., Digital coronagraph algorithm, *OSA Continuum,* 2018, vol. 1, no. 2, pp. 625–633.